

# Mechanical behaviour of Timber-concrete composite façade under temperature

Roufaida ASSAL, Laurent Michel, Emmanuel Ferrier

*Laboratory of Composite Material for Construction, LMC2  
University Claude Bernard Lyon 1,  
82 bd Niels Bohrs, Villeurbanne, 69622, FRANCE*

## Summary

This study aims to address a new concept of structure: the adhesive-bonded wood-concrete façade, referred to as "Hybrimur." Investigating the thermomechanical behavior of wood-concrete façade panels is crucial for several reasons. Firstly, the temperature fluctuations these panels undergo can generate significant thermal stresses within the materials and at their interfaces, potentially jeopardizing structural integrity and durability. To examine these phenomena, four wood-concrete façade prototypes were subjected to thermal testing. These prototypes included two types of façades: two panels reinforced with fiberglass-reinforced concrete and two panels reinforced with welded mesh. Each prototype had standard dimensions of 3 meters in height and 6 meters in width, with a concrete thickness of 7 cm and a laminated timber (GL24h) thickness of 16 cm. The study includes a thermal analysis focusing on the temperature gradients at the adhesive joint, an analytical component, and a numerical model.

## 1 INTRODUCTION

The concept of timber-concrete composite (TCC) structures was first developed in the early 20th century [1]. TCC systems can support up to 60% more load compared to conventional timber beams, and their increased stiffness, particularly when ultra-high-performance fiber-reinforced concrete (UHP-FRC) is used, helps reduce long-term deformations [2, 3]. Recent industry trends have involved increasing the thickness of exterior walls to improve insulation material installation, with studies such as those by Ge et al. [4] demonstrating significant reductions in heat loss and gain in prefabricated timber wall systems. Comparative studies on materials and construction technologies have revealed significant variations in environmental impact and performance. Pérez-García et al. [5] highlighted that multi-layer structural panels (MSP) incorporating timber reduce material and energy requirements, leading to cost savings and lower CO<sub>2</sub> emissions. This is consistent with the findings of Mascia and Soriano [6], who emphasized the importance of connection stiffness for optimizing the performance of composite systems. Various connection technologies, including discrete, continuous, and adhesive connections, play a crucial role in this optimization. Clouston et al. [6] demonstrated that adhesive connections can provide high stiffness. Previous research has explored the use of hybrid beams combining glued laminated timber (GLT), ultra-high-performance fiber-reinforced concrete (UHPC), and fiber-reinforced polymers (FRP). Ferrier et al. (2010) [7] investigated a hybrid beam concept where the GLT section was reinforced with UHPC on the upper surface of the compressed zone and FRP on the lower surface of the tensioned zone. The results indicated that this combination significantly enhances structural efficiency compared to traditional GLT beams. Ferrier et al. (2012) [8] emphasized the importance of considering combined shear and transverse tensile stresses for hybrid beams, particularly when the span is less than 17 times the height of the beam, to accurately predict deflection. The equations used for GLT beams are also applicable to hybrid beams. The primary challenge of hybrid systems, however, lies in managing thermal stresses induced by temperature differentials, which can lead to panel deformation and bending. This issue is well-documented but not fully understood within civil and mechanical engineering practices [9]. In some cases, these thermal stresses can be as significant as those generated by permanent and live loads, potentially causing concrete cracking, construction challenges, and serviceability issues such as the debonding of façade attachments due to excessive deformation [10]. This

paper presents the results of an experimental program on the thermal stress of glued wood-concrete façade panels. Four full-scale panels (6 meters in length), both with and without insulation, were tested. To the authors' knowledge, few studies have addressed the thermal deformation of insulated façade panels. This study aims to examine the thermal stress of the panels while excluding other factors such as creep, humidity, and connections, which will be explored in future research.

## 2 EXPERIMENTAL TESTS

The wood used in the façade design consisted of glulam elements of strength class GL24H. Table 1 shows the mechanical properties derived from Eurocode 5 EN1994 [11], bending strength  $f_{m,g,k}$ ; tensile strength parallel to the grain  $f_{t,0,g,k}$  compressive strength parallel to the grain  $f_{c,0,g,k}$  shear strength  $f_{v,g,k}$ ; mean modulus of elasticity parallel to the grain  $E_{0,g,05}$ ; and characteristic modulus of elasticity parallel to the grain  $E_{0,g,mean}$ . The external skin of the concrete is strength class C40/50 concrete. The mechanical properties of the concrete are summarized below [12], where  $f_{ck}$ ,  $\epsilon_{cu}$ ,  $E_{cm}$  represent the cylindrical compression strength, strain corresponding to the maximum compression stress, and Young's modulus, respectively. The adhesive used is a two-component epoxy resin (Eponal 371) whose main mechanical properties, as specified by the manufacturer. It is essential to include the specific heat capacity (C) and the density ( $\rho$ ) of the constituent materials, as well as the coefficient of thermal expansion for concrete, wood, and steel. These coefficients are necessary to obtain the mechanical response and have been estimated based on data from the literature. The connection was considered perfect since the thickness of the adhesive joint does not exceed 1 mm. The values of the thermal properties of glued-laminated timber were assessed based on data from the literature [13]. The specific heat capacity and thermal conductivity of concrete are calculated using the equations provided in Eurocode NF EN 1992-1-2:2004 [14]. At ambient temperature, the coefficient of thermal expansion ( $\alpha$ ) of concrete ranges from  $6 \cdot 10^{-6}$  to  $13 \cdot 10^{-6}$  [15].

**Table 1.** Mechanical properties of the materials.

Material	Parameter	Value
Concrete	$f_{ck}$ [MPa]	40.8
	$\epsilon_{cu}$ [%]	0.38
	$E_{cm}$ [MPa]	33 546
	Poisson's ratio ( $\mu$ )	0.2
	Specific heat capacity (C) [KJ/kg K]	840
	Thermal conductivity ( $\lambda$ ) [W /m K]	1.15
	Coefficient of thermal expansion ( $\alpha$ ) [ $K^{-1}$ ]	$10^{-6}$
Timber (GL24h)	$f_{m,g,k}$ [MPa]	24
	$f_{t,0,g,k}$ [MPa]	16.5
	$f_{c,0,g,k}$ [MPa]	24
	$f_{v,g,k}$ [MPa]	2.7
	$E_{0,g,mean}$ [MPa]	11 600
	$E_{0,g,05}$ [MPa]	9400
	Poisson's ratio ( $\mu$ )	0.3
	Specific heat capacity (C) [KJ/kg K]	1600
	Thermal conductivity ( $\lambda$ ) [W /m K]	0.15
Coefficient of thermal expansion ( $\alpha$ ) [ $K^{-1}$ ]	$5.5^{-5}$	
Resin	$f_c$ [MPa]	$83 \pm 4$
	$f_t$ [MPa]	$32 \pm 3$
	$\epsilon_t$ [%]	$1.2 \pm 0.2$
	$E_t$ [MPa]	$3500 \pm 500$

The Poisson's ratio ( $\mu$ ) of the wood is considered constant, with a fixed value set at HR = 12%, to ensure the evaluation of deformations at the interface without introducing any timber stress due to moisture.

## 2.1 Experimental program and Test conditions

The test panel design is depicted in **Fig. 1**. Each panel, fabricated by Cruard company, has dimensions of 6 meters in length and 1.2 meters in width. The panels consist of a 7 cm thick concrete layer and a 16 cm thick timber layer, designed to reduce overall weight and minimize greenhouse gas emissions. Two configurations were evaluated: one incorporating fiber reinforcement and insulation, and another without these components. Fibers were incorporated into the concrete matrix as an alternative to conventional reinforcement techniques. The panels were bonded using Eponal epoxy adhesive, as outlined by **Augeard et al. [9]**. It is important to note that, in practical applications, the timber layer is oriented towards the interior of the building, while the concrete layer is exposed to external environmental conditions.

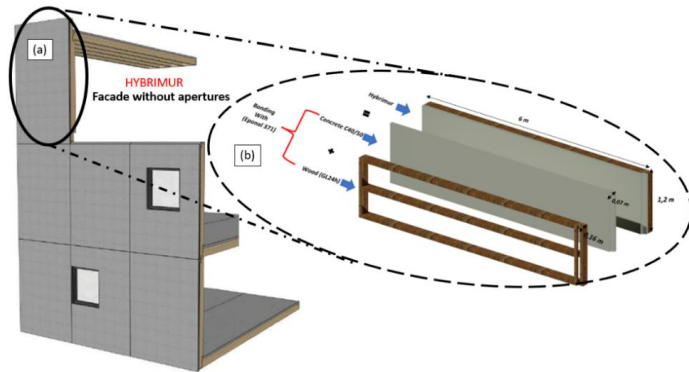


**Fig. 1** Principle of adhesively bonded wood-concrete façade elements with composite structural behavior at (a): the building level, (b): element level.

The testing conditions for this configuration are illustrated in **Fig. 2**. The tests were conducted in a laboratory setting, where two panels were positioned opposite each other to ensure consistent test repeatability and maximize efficiency. During the testing, the wood side of the panels was exposed to ambient air, while the inner concrete surface was heated to 70°C, creating a temperature gradient of 50°C. Upon reaching this temperature, the tests were paused to apply glass wool insulation around the panels, both to evaluate its effectiveness and to achieve a more uniform temperature distribution across the panels. To further optimize the insulation, additional cut panels and insulating foam were placed on top of the heated panels. The cooling phase of each panel was monitored and recorded. After this, the tests were resumed to assess the effect of the insulation on the thermal performance of the façade.

**Table 2.** Panel tested and test conditions.

Tests	Panels	Conditioning	Applied Temperature (°C)		Loading process	Loading duration (Hours)
Test 1	FG-P	Without insulation	65	24	Heating Cooling	50
Test 2	FG-P	Insulated	70	24	Heating	70
Test 3	R-P	Without insulation	63	22	Heating Cooling	28
Test 4	R-P	Insulated	70	26	Heating	70
Test 5	R-P	Insulated	67	22	Heating	62

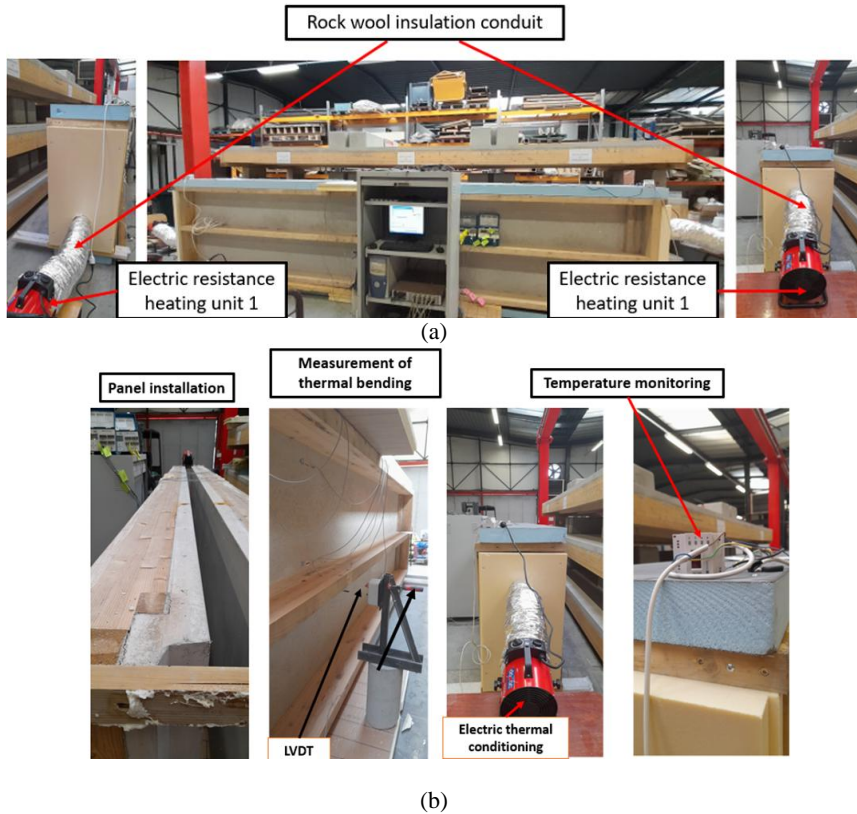
**FG-P: Fiberglass-reinforced panel, R-P: Reinforced Panel (Standard panels).**



Fig. 2. Test conditions: (a) Setup of the tested panels; (b) Installation of the insulation.

## 2.2 Instrumentation

For this study, the panels were subjected to heating using two 3.0 kW electric heaters, each equipped with spiral heating elements. This configuration was chosen to ensure uniform and efficient heat distribution, even in confined spaces. The electric heaters are equipped with an integrated thermostat and an adjustment knob for precise temperature control. They feature a multi-position switch that allows for selection between two heating powers (1.5 kW or 3.0 kW) and a fan mode. The blow angle can be adjusted from 0 to 20°, with an airflow rate of 286 m<sup>3</sup>/h. To optimize heat distribution across the panels, the heaters were positioned at the ends of the panels. Heat transfer to the panels was facilitated through soundproofed rock wool ducts, compliant with standard M1, with a diameter of 200 mm and a length of 10 meters. These ducts effectively channel the hot air while providing sound insulation. The thermal gradient was controlled using the H-Tronic HTS 1000 device. The thermal switch was strategically positioned and connected to the heaters at the ends of the panels to ensure precise regulation of heat distribution. K-type temperature sensors were installed to measure the temperature gradient. One sensor was placed on the concrete exposed to the ambient laboratory temperature (K1), and another sensor was positioned on the heated concrete (K2). This setup allows for accurate monitoring of the thermal gradient variations between the unheated and heated concrete surfaces. All components and their placements in this setup are illustrated in Fig. 3.



**Fig. 3** Instrumentation: (a) Installation of the heating system, (b) Installation of thermal switches and thermocouples.

To evaluate thermal expansion, three 30 mm strain gauges were installed on the wooden sections of the panel. One strain gauge was placed on the cooled concrete, another on the heated concrete, and an additional gauge was positioned on the outer surface of the concrete exposed to the ambient environment. The specific locations of these gauges are illustrated in **Fig. 4**. The following table provides a summary of the gauge locations and their designations on each panel.

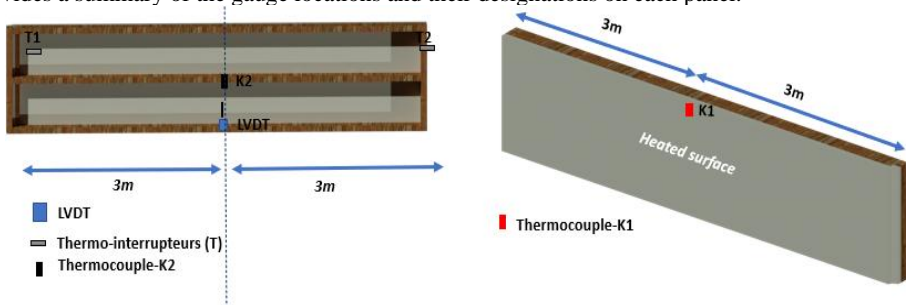


**Fig. 4.** Thermocouples and LVDTs.

### 3 THERMOMECHANICAL MODELING OF PANELS

This section focuses on the development of a finite element model to determine the mechanical response of the panel (strains, deflections, temperature gradient at the interface) under the influence of applied temperatures and induced thermal gradients. The finite element analysis is conducted using Abaqus software, with a fully coupled temperature-displacement study. The results allow the evaluation of the panel's mechanical response based on the applied nodal temperatures.

### 3.1 Numerical Calculation Assumptions

In this analysis, both wood and concrete are considered to behave as isotropic elastic materials. For the bonded assemblies, the interfaces between wood-adhesive and adhesive-concrete are assumed to be perfect, implying no gaps or sliding, and all materials exhibit isotropic elastic behavior that is independent of moisture content. The finite element mesh comprises C3D8T elements (**Fig. 5**), which are 8-node linear bricks that allow for trilinear interpolation of displacements and temperatures. The elements have an approximate size of 3 mm, providing a high level of mesh resolution. This fine mesh size ensures sufficient accuracy, eliminating the need for further mesh refinement studies.

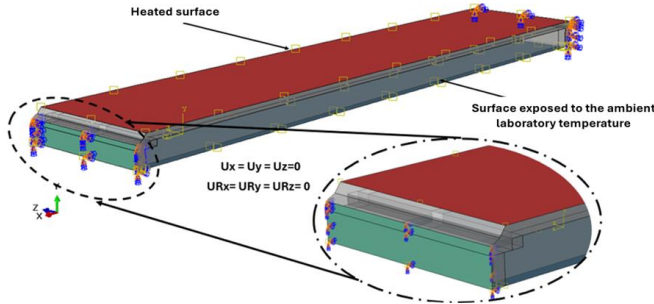


**Fig. 5.** Boundary conditions and applied loading.

For this configuration, tetrahedral elements were selected due to the geometric complexity of the model. All simulations were conducted in three dimensions to closely align with the experimental setup. The boundary conditions, consistent with the experimental setup, involved fixing the panel at the ends, with all displacements and rotations constrained ( $u_x = u_y = u_z = u_{Rx} = u_{Ry} = u_{Rz} = 0$ ) also in accordance with the experimental conditions. Figure 5 illustrates the boundary conditions for both facades.

## 4 RESULTS AND DISCUSSION

**Figures 6** illustrates the vertical displacement along the panel length. All panels exhibit deformation in response to the applied thermal load. Due to the clamped boundary conditions at the ends ( $u_x = u_y = u_z = u_{Rx} = u_{Ry} = u_{Rz} = 0$ ), displacements are constrained to zero at these fixed ends and reach a maximum at 4 meters along the length, as opposed to 3 meters, aligning with the observed structural asymmetry of the panels. Additionally, thermal deflections were measured at the midpoint of the panel's length on the heated side of the concrete. It is also observed from the curves that there is a residual displacement at the free end of the heated panel. The curves show that the panel continues to move, with an amplitude varying from 0.3 mm to 0.5 mm. The results summarized in the table below show discrepancies ranging from 30% to 67% between the numerical and experimental values during thermal dilation tests. Although the maximum deflections observed in each panel remain below the typical limit of  $L/360L$  (16.7 mm) defined by the CSA A23.3 standard, these tests indicate that the deflections reach up to 68% of this limit, without additional load. A detailed observation of the thermal deflection evolution through the three regimes was necessary. It was important to assess the panels' ability to return to their original shape upon cooling. However, for the insulated panels, cooling was not recorded as the test was interrupted before this phase. It is noteworthy that there is considerable variability between numerical and experimental results, as illustrated by the following examples: in the absence of insulation (**Figure 7a**), the measured deflection for the reinforced panel reached 5 mm, compared to 1.9 mm experimentally measured, representing a significant discrepancy of 62%. Similar observations were noted for the fiber-reinforced panel (**Figure 7b**), where the measured deflection was 5 mm experimentally, versus a numerical estimate of 3.6 mm. The addition of insulation in the case of the reinforced panel (**Figure 7c**) reduced the deflection to about 2.1 mm, with a minimal difference of 0.1 mm for the fiber-reinforced panel (**Figure 7b**) between the insulated and non-insulated configurations. For the panels with insulation (**Figure 7d**), the minimal increase in vertical displacement was observed, except during the heating and cooling phases, where 1 mm discrepancies were noted during the transition to the steady-state regime. Another significant observation concerns the isotherms of vertical displacements shown in **Figure 6**. It is noted that, for the uninsulated panels, the maximum deflection occurs primarily near the edges of the panel. In contrast, for the insulated panels, the maximum deflection is

closer to the center of the panel. This phenomenon reflects the thermal distribution in the heated area of the concrete and confirms the hypothesis that displacements are concentrated in the less asymmetric regions of the panel, as illustrated by the displacement isotherms.

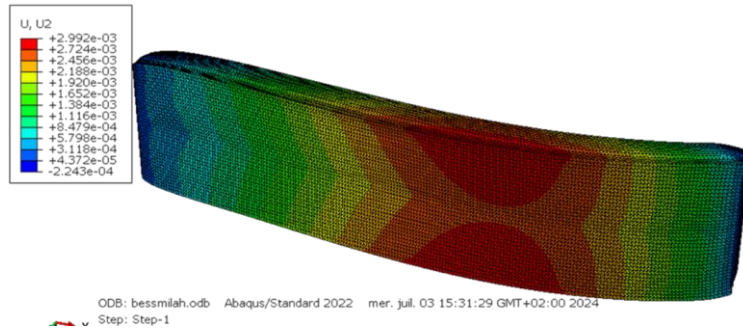


Fig. 6. Deformed shape of the panel.

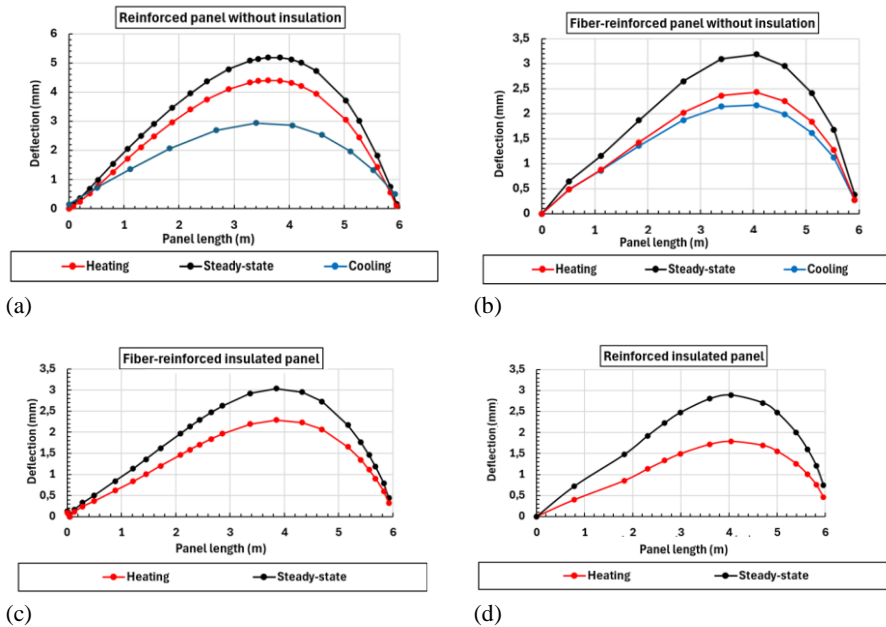


Fig. 7. Deflection at the center of the panel as a function of the panel length: (a) Uninsulated reinforced panel, (b) Uninsulated fiberglass-reinforced panel, (c) Un-sulated reinforced panel, and (d) Un-sulated fiberglass-reinforced panel.

## 5 CONCLUSIONS

In this study, the concrete panels were heated to 70°C while the wooden side was kept at ambient temperature, creating a temperature gradient of 50°C. After reaching this target temperature, tests were paused, and glass wool insulation was applied to evaluate its impact. Temperature Gradient: The temperature gradient varied significantly between the fiber-reinforced and reinforced panels. For the fiber-reinforced panel, the gradient was between 43°C and 48°C without insulation, with only a slight increase of 1°C upon adding insulation. Conversely, the reinforced panel showed a gradient up to 51°C without insulation, which increased by 3°C compared to the fiber-reinforced panel. Insulation reduced the temperature gradient incrementally but remained significant. Impact of Insulation on Thermal Bending: Insulation did not significantly increase the thermal bending of the panels. For the fiber-reinforced

concrete panels, thermal bending only slightly increased with insulation, from 4.4 mm to 4.8 mm for Panel P1 and from 5 mm to 5.6 mm for Panel P2. Panels 3 and 4 exhibited a gradual increase in bending, which accelerated due to thermal lag from insulation. Without insulation, displacements were similar across panels, with Panels 3 and 4 showing relatively low deflections due to mid-span thermal response. Experimental deflections for 6-meter panels reached a maximum at about 4 meters, with discrepancies between numerical and experimental measurements ranging from 30% to 67%. Deflections were often greater experimentally, with differences up to 62% for uninsulated reinforced panels. Insulation reduced deflections, notably for the reinforced panel, with minimal difference observed for the fiberglass-reinforced panel.

### Acknowledgement

The authors would like to express their gratitude to the French agency ADEME for the financial support of the Hybrid 2 project, and to the companies CRUARD Charpente and Jousselin for their assistance in preparing the test specimens.

### References

- [1] F. E. Richart et C. B. Williams, « Tests of composite timber and concrete beams », University of Illinois Engineering Experiment Station bulletin; no. 343, 1943.
- [2] J. E. Augéard, L. Michel, et E. Ferrier, « Experimental and analytical study of the mechanical behavior of heterogeneous glulam–concrete beams and panels assembled by a specific treatment of wood », *Construction and Building Materials*, vol. 191, p. 812-825, 2018. <https://doi.org/10.1016/j.conbuildmat.2018.10.038>.
- [3] S. V. Glass et S. L. Zelinka, « Moisture relations and physical properties of wood. Wood handbook: wood as an engineering material: chapter 4. Centennial ed », General technical report FPL, p. 4-1, 2010.
- [4] H. Ge et F. Tariku, « Evaluation of the thermal performance of innovative pre-fabricated wall systems through field testing », in *Proceedings of Building Enclosure Science & Technology (BEST3) Conference, Atlanta (USA), 2012*. T. J. Sorensen, R. J. Thomas, S. Dorafshan, et M. Maguire, « Thermal bridging in concrete sandwich walls », 2018.
- [5] J. A. Perez-Garcia, A. G. Villora, et G. G. Pérez, « Building's eco-efficiency improvements based on reinforced concrete multilayer structural panels », *Energy and buildings*, vol. 85, p. 1-11, 2014. <http://dx.doi.org/10.1016/j.enbuild.2014.08.018>.
- [6] J. P. Clouston et A. Schreyer, « Design and use of wood–concrete composites », *Practice Periodical on Structural Design and Construction*, vol. 13, no 4, p. 167-174, 2008. [https://doi.org/10.1061/\(ASCE\)1084-0680\(2008\)13:4\(167\)](https://doi.org/10.1061/(ASCE)1084-0680(2008)13:4(167)).
- [7] J. E. Ferrier, P. Labossière, et K. Neale, « Mechanical behavior of an innovative hybrid beam made of glulam and ultrahigh-performance concrete reinforced with FRP or steel », *Journal of Composites for Construction*, vol. 14, no 2, p. 217-223, 2010. [https://doi.org/10.1061/\(ASCE\)CC.1943-5614.0000063](https://doi.org/10.1061/(ASCE)CC.1943-5614.0000063)
- [8] J. E. Ferrier, P. Labossière, et K. Neale, « Modelling the bending behaviour of a new hybrid glulam beam reinforced with FRP and ultra-high-performance concrete », *Applied Mathematical Modelling*, vol. 36, no 8, p. 3883-3902, 2012. [doi:10.1016/j.apm.2011.11.062](https://doi.org/10.1016/j.apm.2011.11.062).
- [9] V. F. Leabu, « Problems and performance of precast concrete wall panels », in *Journal Proceedings*, 1959, p. 287-298.
- [10] Y. Mai, « Performance evaluation of sandwich panels subjected to bending compression and thermal bowing », *Matériaux et Construction*, vol. 13, p. 159-168, 1980.
- [11] EN 1995-1-1:2004 Eurocode 5: Design of timber structures - Part 1-1: General - Common rules and rules for buildings
- [12] F. Dunlap, *The specific heat of wood*, vol. 110. US Department of Agriculture, Forest Service, 1912.
- [13] A. TenWolde, J. D. McNatt, et L. Krahn, « Thermal properties of wood and wood panel products for use in buildings », Forest Service, Madison, WI (USA). Forest Products Lab., 1988.
- [14] EN 1992-1-2 (2004) (English): Eurocode 2: Design of concrete structures - Part 1-2: General rules - Structural fire design
- [15] M. I. Khan et M. Karahan, « Testing of Natural Fiber Composites », in *Natural Fibers to Composites: Process, Properties, Structures*, Springer, 2022, p. 131-148.